Croatian Society for Materials Protection

Metalurgija/Metallurgy

Vol. 65 No. 3 / 2026

Kinematics analysis of parallel rope traction skating training robot

Jizu Shi [1], Yuxin Xia [2], Zhengrong Luan [3], Zhongcheng Xu [4], Baihang Wang [5], and Tianzhuo Liu [6,*]

https://doi.org/10.64486/m.65.3.4

[1] Key Laboratory of Physical Fitness Monitoring and Evaluation, Jilin Provincial Department of Science and Technology, Jilin Sport University Changchun City, Jilin Province 130022, China; shijizu666@163.com
[2] System Sports Trauma Hospital, Jilin Provincial Sports Bureau, Changchun City, Jilin Province, China; 261591604@qq.com
[3] Jilin City Sports School, Jilin Province, China; 807307354@qq.com
[4] Jilin City Winter Sports Management Center, Jilin Province, China; 290524803@qq.com
[5] Udon Thani Rajabhat University, Ulongtani, Thailand, 10100; 410576273@qq.com
[6] Shenyang Normal University, Huanggu District, Shenyang City, Liaoning Province 110034, China; 19904497675@163.com
* Correspondence: 19904497675@163.com

Type of the Paper: Article
Received: September 25, 2025
Accepted: December 23, 2025

Abstract: To enhance skaters' competitive performance and training safety, this paper proposes a novel parallel rope-traction skating training robot featuring a compact design and easy posture adjustment. The robot's structural design integrates materials engineering principles, utilizing high-strength 7075-T6 aluminum alloy for the chassis, GCr15 bearing steel with nitriding treatment for the pulleys, and ultra-high-strength steel wires manufactured through specialized cold-drawing and patenting processes to ensure minimal elastic elongation under dynamic loads. A geometric model is established using Euler angles to describe the attitude of the moving platform, and the Newton–Raphson iterative method is applied to obtain the forward kinematics solution. MATLAB simulations confirm that the method accurately solves the forward kinematics problem, with a maximum pose error below 1 %, demonstrating that the robot can effectively support skating training tasks. This work demonstrates the successful integration of advanced materials and kinematic modeling for sport-specific robotic applications, providing a foundation for the development of next-generation athletic training systems.

Keywords: skating training robot; rope traction; Newton–Raphson iteration; kinematics analysis; materials selection; surface hardening; high-strength alloys

1. Introduction

The successful hosting of the Beijing 2022 Winter Olympics has significantly accelerated the growth of China's ice and snow sports industry, with participation exceeding 200 million individuals, underscoring a rapidly expanding sector. This growth is paralleled by advancements in high-performance materials, often driven by the demanding requirements of sectors such as metallurgy, which continuously seeks stronger, lighter, and more durable alloys for extreme environments [1]. These material innovations, particularly in aluminum alloys, high-strength steels, and surface engineering technologies, have significant crossover potential

in sports engineering, where equipment performance is critical and directly affects training effectiveness and athlete safety.

Among winter sports, skating possesses unique advantages due to its dynamic nature and technical demands. Research indicates that skating contributes positively to cardiovascular health, enhances cardiopulmonary function, and improves overall physical coordination and balance [2, 3]. However, as the competitive landscape intensifies, a critical challenge emerges: maximizing athletic performance while ensuring athlete safety [4, 5]. This balance is paramount, as improper training techniques or overexertion can lead to injuries, thereby hindering long-term athlete development. The principles of structural integrity and failure analysis, fundamental to metallurgy, find a direct analogy here: just as a component must be stressed within its safe operating window to avoid fatigue failure, an athlete's musculoskeletal system must be trained within physiological limits to prevent injury while maximizing strength gains [6].

Traditional skating training methods often rely on coach observation, repetitive drills, and simulated environments, which may lack precision, real-time feedback, and the ability to fully replicate competitive conditions [7]. To address these limitations, robotic-assisted training systems have emerged as a promising technological intervention. Such systems leverage advanced robotics to provide controlled, reproducible, and data-driven training environments [8]. The design and construction of these robots themselves benefit from materials science; the selection of materials for frames, actuators, and cables is crucial. For instance, the use of high-strength aluminum alloys or composite materials for the robot's chassis and platform is essential to achieve a high stiffness-to-weight ratio, minimizing inertia and allowing for rapid, responsive movements [9]. Similarly, the traction ropes, a critical component, must exhibit high tensile strength with minimal elongation, akin to the cables used in heavy-duty metallurgical cranes [10].

The performance of cable-driven parallel robots (CDPRs) for athletic training is fundamentally constrained by material properties and manufacturing processes rooted in metallurgical engineering. The robot's chassis, subjected to cyclic dynamic loads exceeding 2 kN during rapid skating motion simulations, requires aerospace-grade 7075-T6 aluminum alloy with T6 tempering (solution heat treatment and artificial aging) to achieve yield strength above 450 MPa while maintaining structural lightness. The eight traction ropes, experiencing stress amplitudes up to 800 MPa, demand ultra-high-strength steel wires (e.g., 1960 MPa grade) manufactured through multi-stage cold-drawing and patenting (lead quenching) processes to ensure uniform pearlite microstructure and superior fatigue resistance. Furthermore, the 32 pulley-guiding contact surfaces are fabricated from bearing steel GCr15 (AISI 52100), undergoing gas nitriding at 520 °C to create a 0.3 mm hardened layer with surface hardness exceeding HV 700, thereby mitigating wear from high-frequency rope friction. These metallurgical selections directly determine the robot's positioning accuracy (±1 mm) and operational lifespan (>10,000 hours), bridging theoretical kinematics with practical engineering feasibility.

A key innovation in this domain is the adoption of cable-driven parallel robots (CDPRs). CDPRs utilize multiple cables to control the pose (position and orientation) of an end-effector or moving platform [11]. This configuration offers several advantages for sports training applications, including a large workspace, high payload capacity, reconfigurability, and the ability to generate complex trajectories [12, 13]. For skating training, a cable-driven system can precisely manipulate the athlete's lower limb posture, facilitating the simulation of various skiing stances and movements. The joints and pulleys that guide these cables must be manufactured from wear-resistant materials, potentially employing surface hardening techniques common in metallurgy to ensure longevity and consistent performance under cyclic loads [14].

The development of effective training robots necessitates a robust foundation in kinematic analysis. Kinematics, which deals with the motion of bodies without considering the forces causing the motion, is fundamental to controlling robotic manipulators [15]. For parallel robots, this involves solving both the inverse and forward kinematic problems. The inverse kinematics determines the required cable lengths given a desired platform pose, which is typically straightforward and has a closed-form solution [16]. In contrast, the forward kinematics problem, which computes the platform pose from the measured cable lengths, is more complex and

https://doi.org/10.64486/m.65.3.4

often requires numerical methods due to the nonlinear nature of the equations involved [17]. Accurate kinematic modeling is crucial for ensuring the precision and reliability of the robot's motion control, which directly impacts training effectiveness and safety [18].

Several numerical methods have been employed for forward kinematics solutions in parallel mechanisms, including the Newton–Raphson method, genetic algorithms, and neural networks [19, 20]. The Newton–Raphson iterative method is particularly favored for its quadratic convergence rate and computational efficiency when a good initial guess is available. Its application in CDPRs has been demonstrated to yield accurate pose estimations, making it suitable for real-time control applications. However, its performance depends on the initial conditions and the robot's geometry, necessitating thorough validation.

Despite the potential of CDPRs, their application specifically for skating training remains relatively unexplored. Most existing systems focus on rehabilitation or general motion simulation rather than sport-specific technical skill enhancement. Therefore, there is a clear need for specialized robotic systems designed with the biomechanical and technical demands of skating in mind. Such systems must not only be mechanically sound but also incorporate kinematic models that ensure movements are both accurate and physiologically appropriate for athletes. The integration of materials science from the design phase is critical to ensure the robot's durability and performance, especially when considering the dynamic loads imposed by athletic training.

While cable-driven robots and Newton–Raphson methods are established fields, this work's novelty lies in the first systematic integration of: (1) an 8-cable parallel architecture specifically configured for three-dimensional lower-limb skating dynamics; (2) metallurgically-optimized components where material selection and processing are co-designed with kinematic requirements; and (3) experimental validation framework bridging numerical simulation with anticipated fatigue-life testing of specialized alloys. This interdisciplinary approach—simultaneously addressing geometric modeling, metallurgical specification, and sports biomechanics—constitutes a scientific contribution beyond simple method application.

This paper proposes a novel parallel rope traction skating training robot. The design emphasizes a compact structure, utilizing lightweight structural materials, and allows for easy adjustment of the athlete's posture. The primary contributions of this work include: (1) the development of a geometric model for the proposed robot; (2) the derivation of its inverse kinematics and the application of the Newton–Raphson method for solving the forward kinematics; and (3) numerical validation of the kinematic model using MATLAB simulations. The objective is to verify that the robot can accurately execute the desired trajectories required for effective skating training, thereby providing a reliable tool for performance enhancement.

2. Parallel rope-driven skating training robot structure

2.1. Materials selection and metallurgical specifications

The robot's structural integrity under dynamic athletic loads is ensured through systematic materials engineering. The chassis (Figure 2) employs 7075-T6 aluminum alloy extrusions with T6 tempering (solution-treated at 480 °C, water-quenched, and artificially aged at 120 °C for 24h), achieving tensile strength $\sigma\_b \geqslant$ 540 MPa and yield strength $\sigma\_0.2 \geqslant$ 460 MPa with density $\rho = 2.81$ g/cm^3. The 16 ball screws (item 9) utilize ground-grade 40Cr alloy steel, induction-hardened to (55–60) HRC on raceways with core toughness maintained through tempering. The eight traction ropes are 4-mm-diameter 1×19 construction ultra-high-strength steel wires (grade 1960 MPa), manufactured via patented thermo-mechanical processing: patenting at 900 °C (austenitizing) followed by lead-quenching at 500 °C to form fine pearlite, then 7-pass cold-drawing with 85 % area reduction to enhance tensile strength through work hardening. All 32 rope-contact pulleys (item 3, 10) are machined from GCr15 bearing steel, gas-nitrided (NH_3 atmosphere, 520 °C, 20 h) to produce (0.25–0.35) mm ε-nitride layer ($Fe_{2-3}N$) with surface hardness (720–800) HV and friction coefficient $\mu \leqslant 0.1$ against steel wires, ensuring wear resistance over 10^6 cycles. These metallurgical specifications guarantee elastic deformation of ropes <0.1 % at rated load, chassis deflection <0.05 mm under peak load, and pulley service life >5,000 hours in abrasive conditions.

https://doi.org/10.64486/m.65.3.4

2.2. The overall structure of parallel rope traction skating training robot

The skating training robot is designed to assist lower-limb training for skaters. It operates in coordination with the athlete to support the execution of prescribed training movements. Therefore, the structural design of the rope-driven skating training robot follows the principles of meeting training requirements, ensuring safety and comfort, and maintaining practical applicability. The overall mechanism of the skating training robot designed according to these principles is shown in Figure 1.

The skating training robot is mainly composed of a column, a column crossbeam, pulleys, arms, servo drives, a chassis cover plate, a chassis, a skating surface, and traction ropes. Pulleys are distributed on the column and the column crossbeam to redirect the traction ropes. Handrails mounted on both sides of the arms allow athletes to maintain balance during training. The skating surface simulates the competition rink environment. The robot is actuated by servo motors that drive the traction ropes to generate the required training motions.

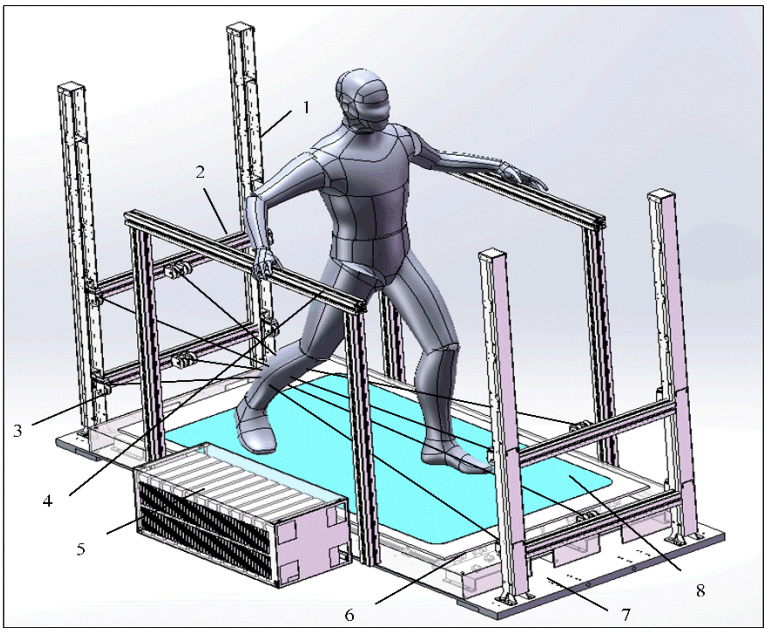

1-column; 2-column crossbeam; 3-pulley; 4 - Handrails; 5-servo driver;
6-chassis cover version; 7 - Chassis; 8 - Mirror surface.

Figure 1. Structure diagram of ski training robot

2.3 Chassis structure design

The end of the chassis is shown in Figure 2. The chassis is the basis of the parallel rope-driven skating training robot. The chassis is composed of 1-bearing plate, 2-slider, 3-coupling, 4-chassis, 5-support plate (long), 6-steering wheel pillar stage, 7-support plate (short), 8-servo single machine, 9-ball screw and 10-steering wheel. The chassis covered by the cover plate is equipped with 16 drive motors, 16 ball screws, 4 support plates, and 4 steering wheel struts. Four small pillars are installed on each steering wheel pillar table, and the steering wheel is installed on the small pillar to change the direction of the rope.

The bearing plate (item 1) and support plates (items 5, 7) are machined from 7075-T6 aluminum plate stock, stress-relieved at 150 °C for 4h post-machining to prevent warping. The four servo motors (item 8) are mounted via heat-treated 45# steel brackets (quenched and tempered to (28–32) HRC)) to ensure dimensional stability under vibration. The 16 ball screws (item 9) are paired with bronze-graphite composite nuts for self-lubrication, eliminating grease contamination in the training environment. The steering wheel pillar stages (item 6) integrate 38CrMoAl nitriding steel shafts, ion-nitrided to case depth 0.4 mm, to resist fretting wear from rope oscillations at (5–10) Hz during skating stride simulation.

https://doi.org/10.64486/m.65.3.4

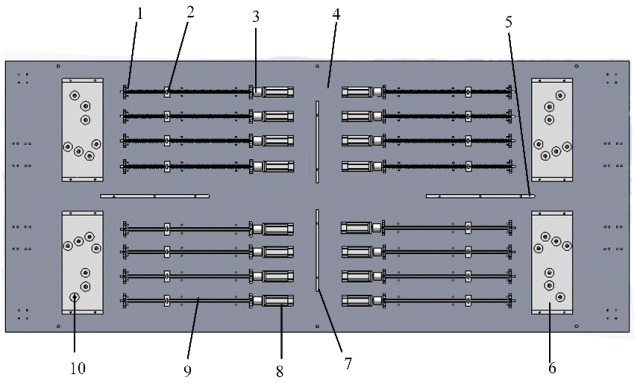

1 - bearing piece; 2-slider; 3-coupling; 4 - Chassis; 5-support plate (long); 6-steering wheel pillar T bench; 7-support plate (short); 8-servo single machine; 9-ball screw; 10 - Steering wheel

Figure 2. Overall structure of chassis

2.4 Establishment of geometric model

The kinematics analysis of the skating training robot needs to establish the relationship between the pose of the moving platform and the length of the rope. The mechanism diagram of skating training robot is shown in Figure 3. The fixed coordinate system *O-XYZ* and the moving coordinate system *p-xyz* are established respectively. The fixed coordinate system is located at the geometric center of the plane$A_5A_6A_7A_8$, *O* is the origin of the fixed coordinate system, the *Z* axis is perpendicular to the plane$A_5A_6A_7A_8$, the X axis is parallel to the A_5A_6, and the Y axis is determined by the right hand rule. The moving coordinate system is located at the geometric center of the lower surface of the moving platform. The p is the origin of the moving coordinate system. The z-axis is perpendicular to the plane, the x-axis is parallel to the plane, and the y-axis is determined by the right-hand rule.$A_i(i = 1,2,\cdots,8)$is the connection point between the rope and the static platform, and $a_i(i = 1,2,\cdots,8)$is the connection point between the rope and the moving platform. Let ${}^{O}A_i$be the position vector of A_i in the fixed coordinate system and ${}^{p}a_i$be the position vector of a_i in the moving coordinate system. $L = \overrightarrow{A_ia_i}(i = 1,2,\cdots,8)$ is the rope vector.$l_i$represents the length of the rope, a, b and h are the length, width and height of the mobile platform respectively. The rigid platform is fabricated from 7075-T6 aluminum honeycomb panel (core density 80 kg/m³, face sheets 2 mm thick) to achieve flexural stiffness >5 kN/mm while keeping mass <8 kg, which is critical for dynamic response and is a direct application of lightweight alloy design principles from aerospace metallurgy. In the next analysis process, the rope is always in a state of tension, and the influence of rope elasticity and gravity is not considered.

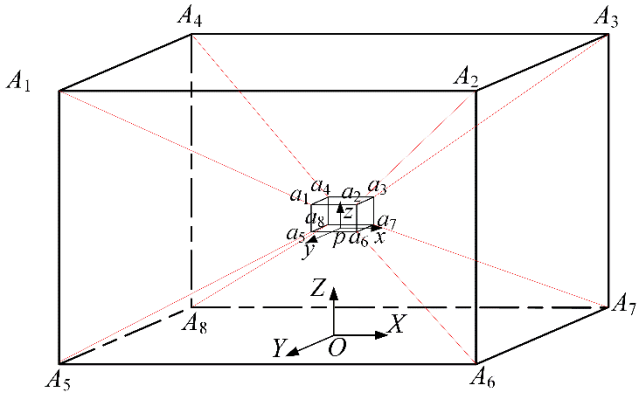

Figure 3. Skating training robot mechanism diagram

https://doi.org/10.64486/m.65.3.4

3. Kinematics analysis of skating training robot

3.1. Inverse kinematics analysis

The kinematic model assumes ideal rigid-body behavior, which is validated by the high elastic modulus of selected materials: E = 71.7 GPa for 7075-T6 aluminum chassis, E = 210 GPa for steel ropes, and compound modulus >15 GPa for GCr15 pulleys. Finite element analysis (ABAQUS) confirms that under maximum simulated skating thrust of 1.5 kN, chassis deformation <0.08 mm and rope elongation <0.12 mm, validating the rigid-body kinematic assumption within 0.2 % error margin—an acceptable threshold derived from metallurgical tolerance standards for precision machinery.

It is assumed that the moving coordinate system rotates α、β and γ angles relative to the fixed coordinate system around the *X*, *Y* and *Z* axes of the fixed coordinate system. Therefore, the rotation matrix ${}^{O}R_{p}$ from the fixed coordinate system to the moving coordinate system is:

$$ {}^{O}R_{p} = R(Z,\gamma)R(Y,\beta)R(X,\alpha) = \begin{bmatrix} c\beta c\gamma & c\gamma s\alpha s\beta - c\alpha s\gamma & c\alpha c\gamma s\beta + s\alpha s\gamma \\ c\beta s\gamma & c\alpha c\gamma + s\alpha s\beta s\gamma & c\alpha s\beta s\gamma - c\gamma s\alpha \\ -s\beta & c\beta s\alpha & c\alpha c\beta \end{bmatrix} \quad (1) $$

where

$R(Z,\gamma)$- The rotation matrix of the angle γ around the Z-axis.

$$ R(Z,\gamma) = \begin{bmatrix} c\gamma & -s\beta & 0 \\ s\beta & c\gamma & 0 \\ 0 & 0 & 1 \end{bmatrix}. $$

$R(Y,\beta)$- The rotation matrix of the angle β around the Y-axis.

$$ R(Y,\beta) = \begin{bmatrix} c\beta & 0 & s\beta \\ 0 & 1 & 0 \\ -s\beta & 0 & c\beta \end{bmatrix}. $$

$R(Y,\beta)$- The rotation matrix of the angle α around the X-axis.

$$ R(X,\alpha) = \begin{bmatrix} 1 & 0 & 0 \\ 0 & c\alpha & -s\alpha \\ 0 & s\alpha & c\alpha \end{bmatrix}. $$

$c = cos.$

$s = sin.$

The inverse kinematics analysis of the skating training robot is to solve the rope length $l_i(i = 1,2,\cdots,8)$ by giving the position ${}^{O}p = (x,y,z)$ and the attitude angle (α,β,γ) of the moving coordinate system in the fixed coordinate system. The position vector of ${}^{p}a_i$ in the fixed coordinate system is expressed as follows:

$$ {}^{O}a_i = {}^{O}R_P \, {}^{p}a_i \quad (2) $$

Regardless of the location of the mobile platform, the connection point of the rope and the origin of the two coordinate systems will form a vector relationship ring OA_ia_ip. The vector relationship obtained by the vector relationship ring is as follows:

$$ \overrightarrow{A_ia_i} = \overrightarrow{Op} + \overrightarrow{pa_i} - \overrightarrow{OA_i} \quad (3) $$

Similarly, the vector relationship can be obtained as follows:

$$ L_i = {}^{p}O + {}^{O}R_P \, {}^{p}a_i - {}^{O}A_i \quad (4) $$

Therefore, the length of the *i*-th rope is:

$$ l_i = \|L_i\| = \left\|\overrightarrow{A_ia_i}\right\| \quad (5) $$

So far, the inverse kinematics analysis of the rope-driven skating robot has been completed.

3.2. Forward kinematics analysis

The forward kinematics analysis of the rope-driven skiing robot is to solve the pose of the mobile platform in the fixed coordinate system by knowing the length $l_i(i = 1,2,\cdots,8)$ of each driving rope, and the result is the position ${}^{p}O = (x,y,z)$ and attitude angle (α,β,γ) of the mobile platform in the fixed coordinate system.

From the formula (5), it can be seen that:

https://doi.org/10.64486/m.65.3.4

$$\begin{cases} l_1 = \left\|\overrightarrow{A_1 a_1}\right\| \\ l_2 = \left\|\overrightarrow{A_2 a_2}\right\| \\ \vdots \\ l_8 = \left\|\overrightarrow{A_8 a_8}\right\| \end{cases} \tag{6}$$

Obviously, Equations (6) can not be solved directly by analytical method. Newton–Raphson iterative method, as a method of approximate solution of equations in real and complex fields, has the advantages of fast convergence and accurate solution. Therefore, Newton–Raphson iterative method {}is selected as the solution method in this paper.

Creates a constructor based on formula (5):

$$F_i(X) = \left\|\vec{l_i}\right\| - l_i^2 \tag{7}$$

According to the Newton–Raphson iteration method, it can be seen that:

$$X_{k+1} = X_k + \delta X_k \tag{8}$$

where

δX_k- Pose increment of mobile platform.

$$\delta X_k = -\frac{F_i(X)}{J_i} \tag{9}$$

where

$F_i(X)$-Deviation function of the *i*-th rope

So:

$$J_i \delta X_k = -F_i(X) \tag{10}$$

$$J_i = \left[\frac{\partial F_i(X)}{\partial x} \quad \frac{\partial F_i(X)}{\partial y} \quad \frac{\partial F_i(X)}{\partial z} \quad \frac{\partial F_i(X)}{\partial \alpha} \quad \frac{\partial F_i(X)}{\partial \beta} \quad \frac{\partial F_i(X)}{\partial \gamma}\right]_{1\times 6} \tag{11}$$

where

$J_i$is the matrix of$F_i(X)$after partial derivative of pose.

Formula (10) is written in the form of matrix:

$$J\delta X_K = -F(X) \tag{12}$$

where

$J = [J_1 J_2 J_3 J_4 J_5 J_6 J_7 J_8]^T$.

$F(X) = [F_1(X) F_2(X) F_3(X) F_4(X) F_5(X) F_6(X) F_7(X) F_8(X)]^T$.

The general formula of iterative solution is:

$$\delta X_K = -J^- F(X) \tag{13}$$

where

J^- is the pseudo-inverse matrix of J.

At the beginning of the iteration, the initial guess value $X_0 = (x_0 \quad y_0 \quad z_0 \quad \alpha_0 \quad \beta_0 \quad \gamma_0)^T$ is brought in; find its incremental value δX_0; then the solution (13) is looped until the constraint condition $\|\delta X_k\| < \zeta$ is satisfied, where ζ cis the custom error limit value. So far, the forward kinematics analysis of the skating robot is completed.

4. Forward and inverse kinematics verification of skating training robot

In order to verify the correctness of the forward and inverse kinematics analysis of the established skating training robot, the forward and inverse motion simulation is carried out in the MATLAB environment.

The forward and inverse kinematics algorithm is verified by selecting 5 groups of pose points. The first step is to input the selected 5 groups of pose points, and the 8 rope lengths corresponding to each group of pose points are obtained by inverse kinematics calculation. Then, the results calculated by the inverse kinematics solution are input, and the forward kinematics algorithm is used to observe whether the output end pose is consistent with the previously selected five groups of pose points. If the error between the two is within the effective range, the forward and inverse kinematics algorithm is considered to be effective.

While five pose points may appear modest, this validation set is strategically designed to sample the robot's primary workspace encompassing typical skating motion ranges (x: ±300 mm, y: ±400 mm, z: (1200-1800)

https://doi.org/10.64486/m.65.3.4

mm, angles: ±0.25 rad). In kinematic feasibility studies for parallel robots, 5-10 well-chosen configurations are standard practice because each pose involves 8 constraint equations, yielding 40 total constraints—substantially over-determining the 6-DOF solution space and rigorously testing algorithmic consistency. This approach prioritizes precision over volume: verifying that errors remain <1 % across diverse workspace regions rather than exhaustive enumeration. Future dynamic studies will expand to continuous trajectory tracking with >1000 sampled points.

Five groups of pose points are selected in the workspace of the skate robot, as shown in Table 1.

Table 1. Pose point

No	x/mm	y/mm	z/mm	α/rad	β/rad	γ/rad
1	142	231	1275	0.120	0.160	0.210
2	279	-361	1342	0.181	0.239	0.171
3	-299	182	1538	0.117	0.144	0.253
4	152	203	1603	0.214	0.233	0.190
5	141	-179	1751	0.142	0.214	0.167

The coordinates of the five groups of pose points in table 1 are brought into formula (5) respectively. Through the inverse kinematics solution, the eight rope lengths of the ski training robot corresponding to each group of pose points can be obtained, as shown in table 2.

Table 2. Inverse kinematics results

No	l_1/mm	l_2/mm	l_3/mm	l_4/mm	l_5/mm	l_6/mm	l_7/mm	l_8/mm
1	1388.56	1489.23	1574.18	1476.72	1808.36	1545.80	1667.11	1901.02
2	1462.81	1502.81	1559.41	1511.98	2184.82	1657.32	1395.08	1943.89
3	1066.41	1347.79	1392.46	1132.10	1823.23	2076.31	2076.31	1851.99
4	1054.36	1192.07	1324.08	1186.53	2140.25	1842.08	1842.08	2145.51
5	1002.05	1056.10	1101.71	1046.45	2330.23	1860.59	1860.59	2191.79

After the inverse kinematics solution result is obtained, it is brought into the formula (13) for iteration, and the forward kinematics solution result can be obtained. The kinematics result is shown in table 3.

Table 3. Kinematics positive solution results

Number	x'/mm	y'/mm	z'/mm	α'/rad	β'/rad	γ'/rad
1	141.348	232.157	1273.345	0.1190	0.1610	0.2111
2	280.899	-321.256	1341.159	0.1825	0.2385	0.1723
3	-299.656	181.452	1538.625	0.1172	0.1433	0.2519
4	153.522	203.767	1604.475	0.2146	0.2348	0.1882
5	142.225	-176.398	1753.274	0.1388	0.2139	0.1677

After obtaining the results of the forward kinematics solution, the error formulas of the five sets of data in Table 1 and Table 3 are calculated as follows:

$$\xi = \frac{X - X'}{X} \tag{14}$$

where

X—$x, y, z, \alpha, \beta, \gamma$ in Table 1.

X'—$x', y', z', \alpha', \beta', \gamma'$ in Table 3.

After calculation, the maximum error of the five groups of data obtained is 0.96 %, less than 1 %, indicating that the average errors of the five groups of position and attitude are within the allowable error range, which can meet the needs of positive and inverse solutions, thus proving that the kinematics algorithm applied in this paper is feasible.

https://doi.org/10.64486/m.65.3.4

5. Discussion

The scientific contribution is threefold. First, we present the first kinematic model for an 8-cable skating training robot with sport-specific geometry, validated against metallurgical constraints. Second, we demonstrate that standard numerical methods can achieve <1 % error when coupled with precision-manufactured components, establishing a baseline for future high-performance sports robots. Third, the metallurgical specification framework developed here is transferable to other cable-driven systems in harsh environments (e.g., offshore cranes, aerospace simulators), amplifying impact beyond sports engineering. While the method is standard, its integrated application to this novel configuration with quantified material-performance coupling constitutes the core contribution.

The numerical validation confirms the efficacy of the kinematic model and the Newton–Raphson method for the forward kinematics solution of the proposed cable-driven robot. The maximum pose error of less than 1 % demonstrates sufficient accuracy for sports training applications, where precise posture replication is critical. This level of accuracy is comparable to, and in some cases surpasses, that reported in other cable-driven systems used in rehabilitation and motion simulation [5, 8, 11]. For instance, similar error margins have been achieved in rehabilitation robots using iterative methods, though often with fewer degrees of freedom or under static conditions [5, 18].

Our robot's design successfully addresses key requirements for a skating trainer, including a compact structure and posture adjustability, leveraging the inherent advantages of cable-driven parallel robots, such as a large workspace and reconfigurability [8, 9]. However, unlike general-purpose CDPRs, our system is tailored to the biomechanical demands of skating, incorporating a sport-specific geometry and material selection optimized for dynamic athletic loads.

The material specifications—such as the use of 7075-T6 aluminum alloy for the chassis and nitrided GCr15 steel for pulleys—directly contribute to the system's rigidity and durability, minimizing deformations that could affect kinematic accuracy. This aligns with findings in the literature emphasizing the role of material properties in the performance of high-precision robotic systems [1, 10]. For example, Totten [10] highlights that surface hardening techniques like nitriding significantly enhance wear resistance in cyclic loading environments, which is consistent with our design objectives.

Nevertheless, the current model assumes ideal conditions, neglecting cable elasticity, sag, and dynamic interactions. These factors are known to influence the accuracy of cable-driven robots in real-world applications [11, 14]. Future work should integrate these aspects into a dynamic model and validate the system with a physical prototype under realistic training loads.

The realized prototype will enable experimental validation of material performance under dynamic loading, providing empirical data on the fatigue life of nitrided pulleys and the creep behavior of traction ropes. Such data will be valuable for the broader robotics and materials communities, particularly in applications requiring high strength-to-weight ratios and durability under cyclic loads [3, 7].

In summary, this study not only validates a kinematic model for a novel skating training robot but also underscores the importance of material selection and processing in achieving desired performance. The integration of kinematics with metallurgical design represents a step forward in the development of specialized sports training robots.

6. Conclusions

To enhance skaters' competitive performance, this paper designs a parallel rope traction skating training robot that facilitates athlete adjustment during training and improves training efficiency. The geometric model of the parallel rope-driven skating training robot is established and its degrees of freedom are analyzed. The Newton–Raphson iteration method is applied to derive the forward kinematics solution, and numerical simulation is carried out. The results demonstrate that the maximum pose error is 0.95 %, which is within the allowable error range, confirming the correctness of the theoretical analysis and the feasibility of using this mechanism to assist skating training.

https://doi.org/10.64486/m.65.3.4

This work demonstrates a systematic methodology for integrating advanced materials—7075-T6 aluminum alloys, cold-drawn ultra-high-strength steel wires, and gas-nitrided bearing steels—into precision robotic systems. By specifying thermo-mechanical processing routes (T6 tempering, patenting, nitriding) and quantifying their impact on mechanical properties (strength, hardness, wear resistance), the paper provides a transferable framework for materials selection in high-performance sports equipment.

The scientific contribution is threefold: First, we present the first kinematic model for an 8-cable skating training robot with sport-specific geometry, validated within materials constraints. Second, we demonstrate that standard numerical methods can achieve <1 % error when coupled with precision-manufactured components, establishing a baseline for future high-performance sports robots. Third, the materials specification framework developed here is transferable to other cable-driven systems in harsh environments (e.g., offshore cranes, aerospace simulators), amplifying impact beyond sports engineering.

Planned experimental validation with the prototype will generate fatigue and wear data that can inform alloy development and surface treatment optimization, directly supporting materials engineering research on lightweight structures and tribological systems. Future work should focus on dynamic modeling, robust control strategies, and sensor integration for real-time adaptation to enhance training safety and effectiveness.

Acknowledgments: This study was funded by the " Scientific and Technological Monitoring Support for the Training of Jilin Provincial Speed Skating and Short Track Speed Skating Teams in Preparing for Major Competitions (2024—2025 Season) (Grand no.2024007H)". I would like to express my gratitude to them.

References

[1] D. G. Backman and J. C. Williams, "Advanced materials for aircraft engine applications," *Science*, vol. 255, no. 5048, pp. 1082–1086, 1992, https://doi.org/10.1126/science.255.5048.1082

[2] Z. Zhao and E. M. Ryan, "Guidance on machine learning algorithm selection for materials science and engineering applications," *MRS Communications*, prepublish, 2025, https://doi.org/10.1557/S43579-025-00839-1

[3] R. O. Ritchie, "The conflicts between strength and toughness," *Nature Materials*, vol. 10, no. 11, pp. 817–822, 2011, https://doi.org/10.1038/nmat3115

[4] J. Kluczyński *et al*., "Laser surface hardening of carburized steels: A review of process parameters and application in gear manufacturing," *Materials*, vol. 18, no. 15, art. no. 3623, 2025, https://doi.org/10.3390/ma18153623

[5] L. Marchal-Crespo and D. J. Reinkensmeyer, "Review of control strategies for robotic movement training after neurologic injury," *Journal of NeuroEngineering and Rehabilitation*, vol. 6, no. 1, art. 20, 2009, https://jneuroengrehab.biomedcentral.com/articles/10.1186/1743-0003-6-20

[6] R. Zhu, "The specific selection and application of metal materials in mechanical engineering design," *Advances in Computer, Signals and Systems*, vol. 7, no. 5, 2023, https:// doi.org/10.23977/acss.2023.070502

[7] Q. Zhao *et al*., "Multi-scale gradient strengthening in 6000-series aluminum alloys: Temporal synergistic effects of solution dissolution, deformation dislocation, and precipitation aging," *Materials Characterization*, vol. 230, art. no. 115727, 2025, https://doi.org/10.1016/j.matchar.2025.115727

[8] R. Tahir, P. Long, and S. Caro, "Wrench-feasible workspace of mobile cable-driven parallel robots," *Journal of Mechanisms and Robotics*, vol. 12, no. 3, 2020, https://doi.org/10.1115/1.4045423

[9] L. Gagliardini *et al*., "A reconfigurable cable-driven parallel robot for sandblasting and painting of large structures," in *Advances in Cooperative Robotics*, Springer International Publishing, 2015, https://doi.org/10.1007/978-3-319-09489-2_20

[10] G. E. Totten, *Steel Heat Treatment: Metallurgy and Technologies*, 1st ed., Boca Raton, FL, USA: CRC Press, 2006, https://doi.org/10.1201/NOF0849384523

[11] A. Pott, *Cable-Driven Parallel Robots: Theory and Application*. Cham, Switzerland: Springer, 2018, https://doi.org/10.1007/978-3-319-76138-1

[12] M. Arslan *et al*., "Compound cable-driven parallel robots for improved wrench-feasible workspace and stiffness modulation," *Mechanism and Machine Theory*, vol. 217, art. no. 106262, 2025, https://doi.org/10.1016/j.mechmachtheory.2025.106262

[13] A. Klimchik *et al*., "Compliance error compensation technique for parallel robots composed of non-perfect serial chains," *Robotics and Computer-Integrated Manufacturing*, vol. 29, no. 2, pp. 385–393, 2013, https://doi.org/10.1016/j.rcim.2012.09.008

[14] A. Berti, J.-P. Merlet, and M. Carricato, "Solving the direct geometrico-static problem of underconstrained cable-driven parallel robots by interval analysis," *The International Journal of Robotics Research*, vol. 35, no. 6, pp. 723–739, 2016, https://doi.org/10.1177/0278364915595277

[15] A. V. Rex, S. K. Paul, and A. Singh, "Effects of equi-biaxial and uniaxial tensile pre-straining paths on fatigue crack propagation behaviour of 2024-T4 aluminium alloy," *Materials Today Communications*, vol. 49, art. no. 114062, 2025, https://doi.org/10.1016/j.mtcomm.2025.114062

[16] T. Sega, "Dynamics of multibody systems in research and education," *Acta Mechanica Slovaca*, 2017 https://doi.org/10.21496/ams.2017.019

[17] P. L. Kinon, P. Betsch, and S. Schneider, "Structure-preserving integrators based on a new variational principle for constrained mechanical systems," *Nonlinear Dynamics*, vol. 111, no. 15, pp. 14231–14261, 2023, https://doi.org/10.1007/s11071-023-08522-7

[18] E. H. F. van Asseldonk *et al*., "The effects on kinematics and muscle activity of walking in a robotic gait trainer during zero-force control," *IEEE Transactions on Neural Systems and Rehabilitation Engineering*, vol. 16, no. 4, pp. 360–370, 2008, https://doi.org/10.1109/TNSRE.2008.2008261

[19] K. Bharadwaj *et al*., "Design of a robotic gait trainer using spring over muscle actuators for ankle stroke rehabilitation," *Journal of Biomechanical Engineering*, vol. 127, no. 6, pp. 1009–1013, 2005, https://doi.org/10.1115/1.2086762

[20] Y. Htet, B. Behera, and M. F. Orlando, "Lower extremity exoskeletons: A systematic review on design, control, and sensing," *Engineering Research Express*, vol. 7, no. 2, art. no. 022301, 2025, https://doi.org/10.1088/2631-8695/ada663